Revealing Novel Connections Between Space Weather and the Power Grid: Network Analysis of Ground-Based Magnetometer and Geomagnetically Induced Currents (GIC) Measurements

Joseph Hughes[1], Ryan Mcgranaghan[1], Adam Kellerman[2], Jacob Bortnik[3], Robert F. Arrit[4], Karthik Venkataramani[1], Charles H. Perry[4], Jackson McCormick[5], Chigomezyo M. Ngwira [1], Morris Cohen [5]

[1]ASTRA, LLC, 282 Century Place Suite 1000, Louisville, Colorado, USA.
[2]Department of Earth, Planetary, and Space Sciences, University of California, Los Angeles
[3]Department of Atmospheric and Oceanic Sciences, University of California, Los Angeles
[4]Technical Executive, Electric Power Research Institute
[5]School of Electrical Engineering, Georgia Institute of Technology. Atlanta, Georgia, USA

Key Points:

- Using a newly released Geomagnetically Induced Current (GIC) dataset obtained from power grid utilities, the unique connections of GIC to magnetometers are shown through wavelet analysis.
- Deviations from average currents are 1.6 times more likely to occur when there is significant magnetic activity
- Some magnetometers are better indicators of GICs than others. These magnetometers are often not the closest to the GIC nodes.

Corresponding author: Joseph Hughes, jhughes@astraspace.net

Abstract

The growing depth and breadth of available data that span the solar-terrestrial environment place us at a tipping point – the potential of these data is immense but realizing that potential requires a new representation. A new network-based approach to represent data collected by power utilities along with information from the solar-terrestrial connection is used. The progress is generated as part of a new project within the National Science Foundation Convergence Accelerator program: "The Convergence Hub for the Exploration of Space Science (CHESS)." Results are shared from current data provided through the Electric Power Research Institute (EPRI) SUNBURST project linked to magnetometer data from the Super Magnetometer Initiative.

These data are transformed into a network with GIC measurements and magnetometers as the nodes in order to answer a long-standing question: "How much more likely are deviations from the average current when there is active space weather"? To answer this question, periods of active space weather are identified in the magnetometer data, and these are compared to times of DC transients in the GIC data. The probability of a these transients is found to be , on average, 1.6 times higher during periods of active space weather than during quiet times. The most indicative magnetometers of these DC transients are often not the closest to where the GICs are measured.

Plain Language Summary

Geomagnetically Induced Currents (GICs) are harmful effects of space weather that have demonstrated their ability to damage power transformers and disrupt the electrical power grid, yet GIC data are rarely available to space weather researchers. A unique partnership with power grid utilities has led to a new data set of GIC observations for space weather research. This work uses data from GIC nodes as well as magnetometer data from a number of stations around the globe to assess how often space weather causes deviations in GICs, and which magnetometers are the best indicators of these deviations.

1 Introduction

Particles and energy from the sun can travel through interplanetary space and produce myriad impacts on Earth, the near-Earth space environment, and susceptible technology. Collectively, these impacts are known as 'space weather,' and they can have dramatic consequences for our technologically-dependant society (Lanzerotti, 2001; Schrijver et al., 2015). Among the most important, yet ironically, least well specified impacts is that of the electric power grid (Pulkkinen et al., 2017; D. H. Boteler, 2019). The most notable example of the power grid's susceptibility to space weather occurred on 13 March 1989 when anomalous GIC flows at the Hydro-Quebec power grid damaged equipment which caused a 9 hour blackout.

When enhanced space weather activity (e.g., the launch of a coronal mass ejection (CME) or a high speed solar wind stream (HSS) from the Sun) interacts with the Earth's magnetosphere, it produces a chain of complex interconnected physical processes, such as intense electric currents in the Earth's charged upper atmosphere, the ionosphere. Ionospheric currents induce electric currents along long conducting wires on the surface of the Earth, an important example of which is electrical transmission lines. The phenomenon of space weather-induced electric currents in the power grid is known as Geomagnetically Induced Currents (GICs) (Viljanen & Pirjola, 1994; Pirjola, 2000). The challenge of understanding, forecasting, and mitigating GICs is a pressing one for the space weather community because they can disrupt the operation of the power system by overheating power transformers and generating excessive harmonics potentially resulting in the loss of power system equipment(Pulkkinen et al., 2017).

The study of GICs has been driven by widely available magnetometer data from, e.g., the Super Magnetometer Initiative (SuperMAG (Gjerloev, 2009)) to quantify the geomagnetic disturbance due to space weather unified with a model of the Earth conductivity to produce the geoelectric field. The geoelectric field can then be used with a representation of the electrical power grid to calculate induced currents or GICs (Pirjola, 2002; D. Boteler & Pirjola, 2017). Despite the challenges and limitations that come from using assumptions of earth conductivity and plane wave propagation, these approaches have shown reasonable agreement with data. A unique partnership with power grid utilities via the Electric Power Research Institute (EPRI) SUNBURST Project (Lesher et al., 1994; EPRI, 2018a, 2018b) is leveraged to build off this analysis. The SUNBURST project is designed to collect high-quality, readily accessible data related to GICs associated with Geo-Magnetic Disturbances (GMDs). SUNBURST, operating since 1990, provides a sophisticated detection and recording network consisting of more than 50 transformer monitors at substations throughout North America. Current utilization of power utilities' data seldom goes beyond the immediate power network, and their union with relevant space weather data (e.g. solar wind parameters) is a rarity. This work uses direct observations of GICs collected at 10 GIC sensor nodes throughout the United States over the course of 2018 to advance the study of GIC characteristics and their connection to widely available magnetometer data.

This work uses network analysis to link the GIC and magnetometer data. Network analysis (Boccaletti et al., 2006) has been a valuable tool in many fields of research, originating in the social sciences (Milgram, 1967), and finding more recent application in numerous disciplines such as biology, engineering, and geophysics (Tsonis et al., 2006; Donges et al., 2009; Steinhaeuser et al., 2011; Malik et al., 2011). Machine learning, of which network analysis is a subdivision, has been used in the space sciences before e.g. (Camporeale, 2019). The efficacy of network analysis for discovery in space weather has been demonstrated (McGranaghan et al., 2017; Dods et al., 2015, 2017; Orr et al., 2019) and motivates its seminal use with GIC data in this work. Here, the nodes of the network are defined by GIC sensors and ground-based magnetometers. A GIC sensor is defined to be connected to a magnetometer if current spikes at the GIC sensor are more likely if there is significant magnetic activity at the magnetometer. Connections calculated for data from 2018 produce insight into the geophysical significance of the connections, the ability of magnetometer data to describe and predict GIC risk, and the connection to space weather phenomena.

This paper is organized as follows: First the GIC data is discussed in Section 2 by outlining the processing methods to remove persistent trends and establish what constitutes a significant GIC using a statistical z score. Then the likelihood of a significant GIC is aligned with Kp, Magnetic Local Time (MLT), and time of year. Next, the magnetometer data processing is discussed in Section 3 and an example of the wavelet analysis is given for the Boulder magnetometer. The likelihood of magnetic activity is then studied as a function of time, MLT, and location. In Section 4, these two data sets are combined to study the increase in GIC probability if there is magnetic activity using Bayesian statistics. This is done for all GIC sensor - magnetometer pairs, as well as for the two systems in totality. Lastly, summaries and conclusions are listed in Section 5.

2 GIC Data

Data provided through the EPRI SUNBURST project gives the transformer neutral Direct Current (DC) as a function of time. This current is driven by a number of factors such as severe terrestrial weather, system operations such as maintenance and switching components, and space weather. Persistent space weather signatures from the S_q current system (Yamazaki & Maute, 2017) are present in the data which make it difficult to set thresholds for what defines a significant DC transient. As an example, a transient which occurs in an high-current region of the daily cycle will appear larger than one which occurs in a low-current region.

In order to remove the persistent trends in the GIC data, the data are averaged over 30-minute intervals for each day, incorporating data from the same time of day, and from 5 days prior to and after the current day (i.e 11-days of information). The mean and standard deviation (σ of these data are used to construct a Quiet-Day Curve (QDC) of the expected current in the absence of magnetic activity. This technique is used for each available GIC measurement node to produce a QDC DC estimate as a function of time of year and magnetic local time. This information is used to baseline the GIC dataset and distinguish between persistent daily trends and disturbance GIC variations. This technique is explained in further detail in Kellerman et al., (in preparation).

The first five days of September 2018 are shown in Fig. 1. Since each station is unique, the y limits are also unique for each station. There is not continuous data from all the transformers, and there also are not continuous QDCs even when there is data. The blue line is the actual current measured, and the solid orange line is the QDC. Dashed orange lines show the 2 σ bounds from the QDC. Note that the enforced y limits of $\pm 3\sigma$ cut-off some of the most extreme currents.

The analysis requires a robust measure of departure of the current from 'normal' behavior. The variable z is defined as deviation of the measurement from the mean expressed in standard deviations of the mean. Currents with $z > 2$ are considered to be significant DC transients. Throughout the paper, "significant DC transients", "significant transients", "DC transients", and "2σ transients" are all used interchangeably.

$$z = \frac{|I - QDC|}{\sigma_{QDC}} \tag{1}$$

Positing a normal distribution, this definition classifies the most deviant 5% of the data as "significant". It is assumed that this measure represents disruptions driven by geomagnetic activity, but it is acknowledged that this measure may also be affected by non-geomagnetic effects such as instrument maintenance or on/off changes. There exist no flags in the data for such instances, but it is assumed that these represent noise in the accumulated statistics and do not manifest in the final results. These significant DC transients are identified visually in Fig. 1 as times where the blue line exceeds the dashed orange lines.

Consider when, both in time and in Magnetic Local Time (MLT), these significant DC transients occur through the 2D histogram in Fig. 2. The color shows the probability that $z > 2$ at any of the sites as a function of time and MLT. The panel on the right shows the time-averaged probability as a function of just MLT. Significant transients are more probable between 5 and 10 MLT when averaged over the entire year for many of the stations such as We, Bu, and Mo, but not at other sites such as Ru and Sh. These transients are also more probable at some times than others - as evidenced by vertical streaks in the left panel. There are prominent times in early June, late August, and early November. Some of these times are well aligned with Kp.

Next consider not *when* the current spikes occur, but *where* they occur. A map of all but one of the sites with the color and size indicating the probability of a $z > 2$ transient is shown in Fig. 3. The map focuses on southeast continental United States to better show detail, which excludes the Vi station in California. The significant transients occur between 3 and 15% of the time, depending on the station.

3 Magnetometer Data

In addition to the GIC data, magnetometer data is also used. SuperMAG contains data from more than 200 magnetometers, some of which have data gaps. For both the

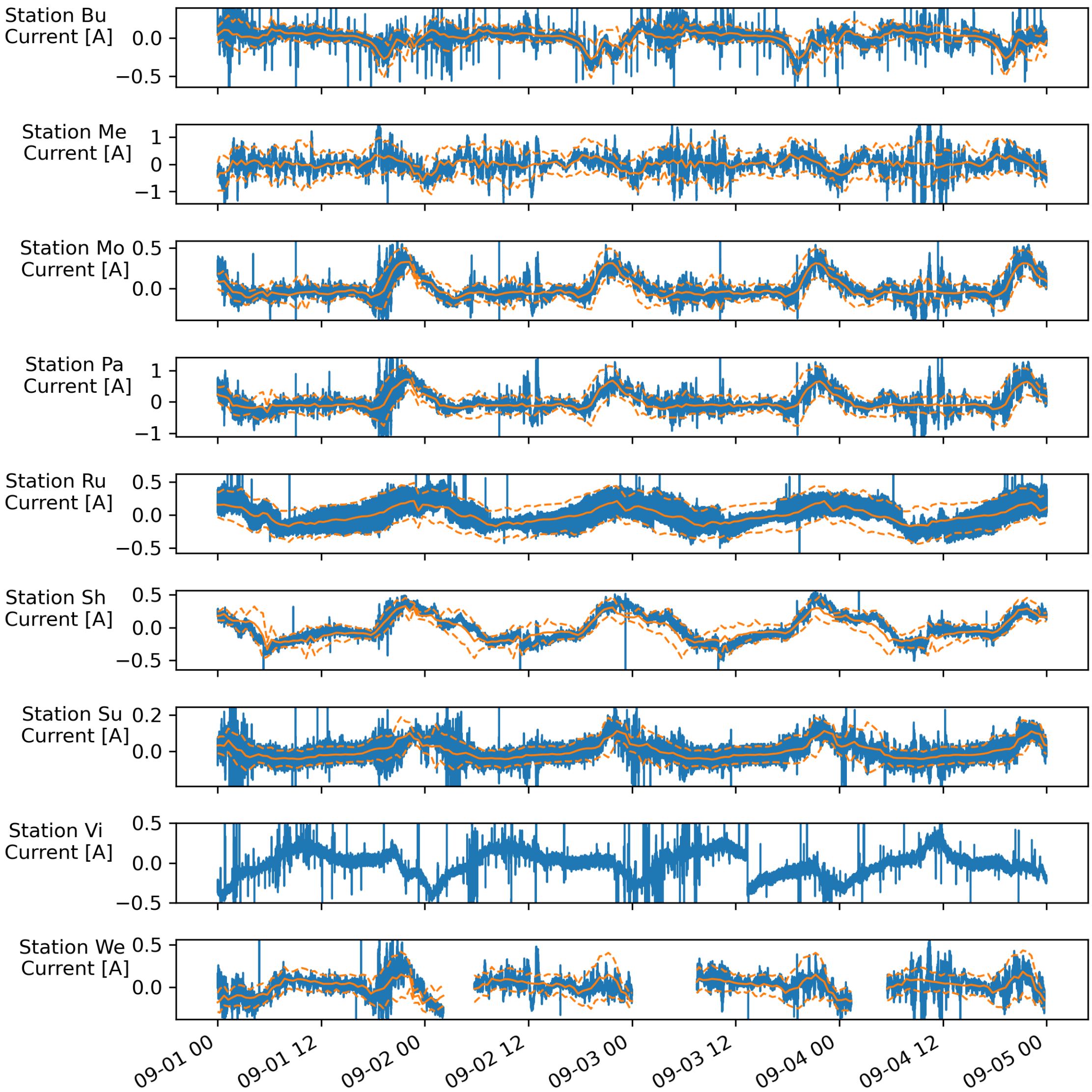

Figure 1. GIC current as a function of time for all stations shown in blue. Solid orange lines show the quiet day curve while dashed lines show the $\pm 2\sigma$ bounds.

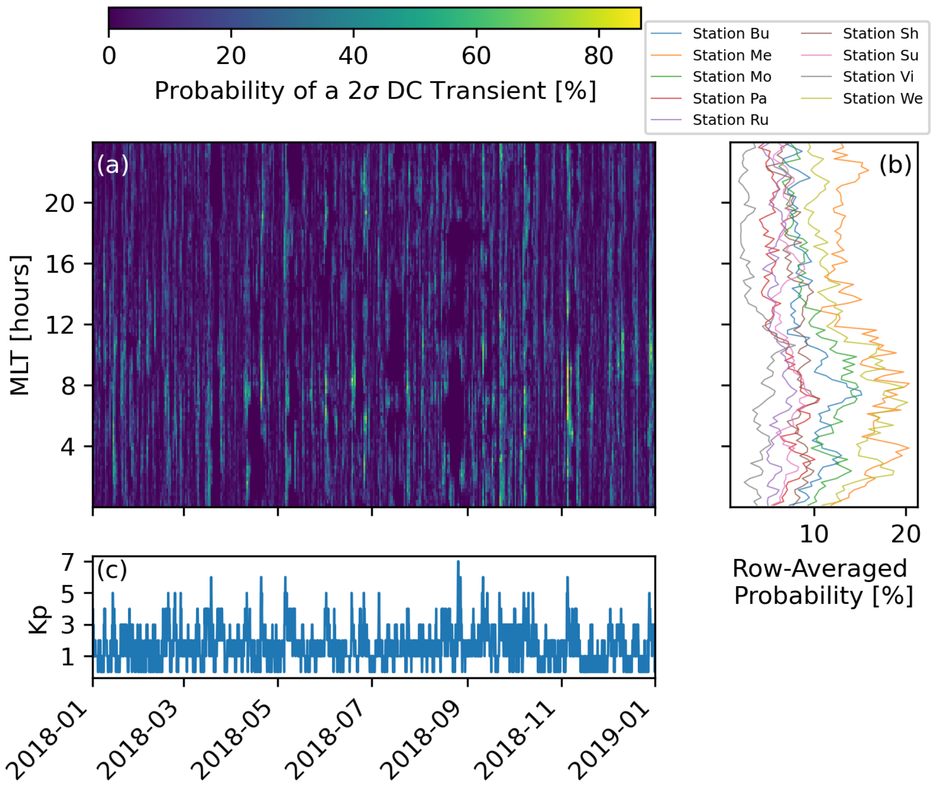

Figure 2. (a) Two dimensional histogram of current spike probability as a function of time and MLT. (b) row-averaged probability histograms just as a function of MLT. (c) K_P as a function of time.

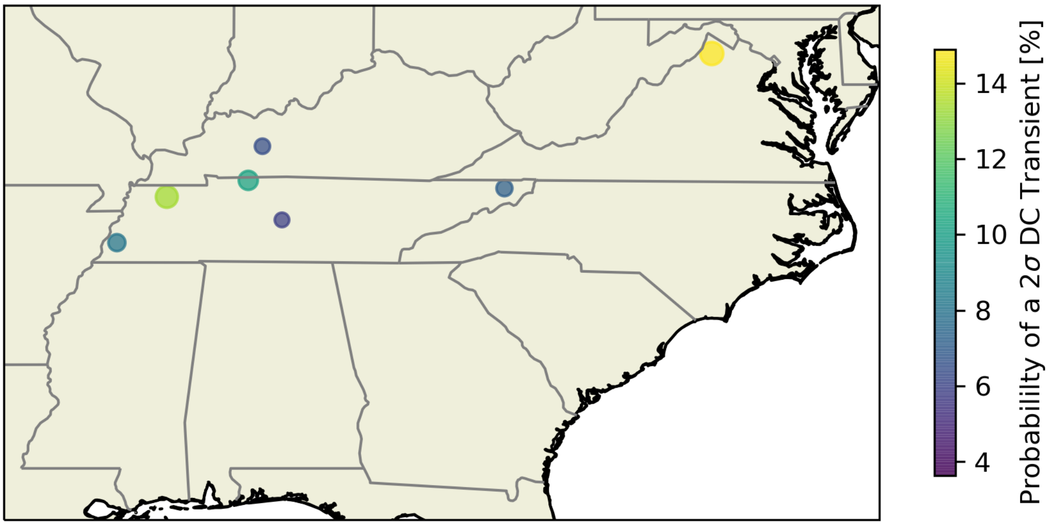

Figure 3. Map of the probability of a 2 σ DC transient at a given site for the whole year. Southeast region shown which omits one west-coast station

GIC data and the magnetometer data, all available data from 2018 is used. The magnetometer data is processed using a wavelet analysis to determine times of statistically significant magnetic activity. Wavelet analysis shows the spectral content of a signal as a function of time. In some ways, it is like a set of Fourier transforms of the signal on different time windows. For this analysis the pycwt python library [1] is used, which is based on (Torrence & Compo, 1998). There are three steps to transform the magnetometer data and they are all shown in Fig. 4 for the Boulder magnetometer.

First, the components of the magnetic field at a given station are converted to a scalar parameter, s:

$$s = \frac{||\boldsymbol{B}(t) - \boldsymbol{B}_m||}{||\boldsymbol{B}_m||} \tag{2}$$

where $\boldsymbol{B}_m$ is the median magnetic field for the whole year. In this analysis, only the horizontal magnetic field (north and east components) are considered since a change in those components induce horizontal electric fields (D. Boteler & Pirjola, 2017), but the results are insensitive to the use of the full field. This may be because the horizontal field is rarely perturbed without the vertical field also being perturbed. A time series plot of the full B field is shown in Fig. 4a, while the scalar parameter s is shown in Fig. 4b.

The second step is to perform a wavelet analysis on s and compute the significance level. This is shown in Fig. 4c, where color indicates the power at the given frequency and time. The dashed black line shows the confidence interval derived from the Nyquist criterion, showing that long-period information spectra be obtained at the beginning or

[1] https://pypi.org/project/pycwt/

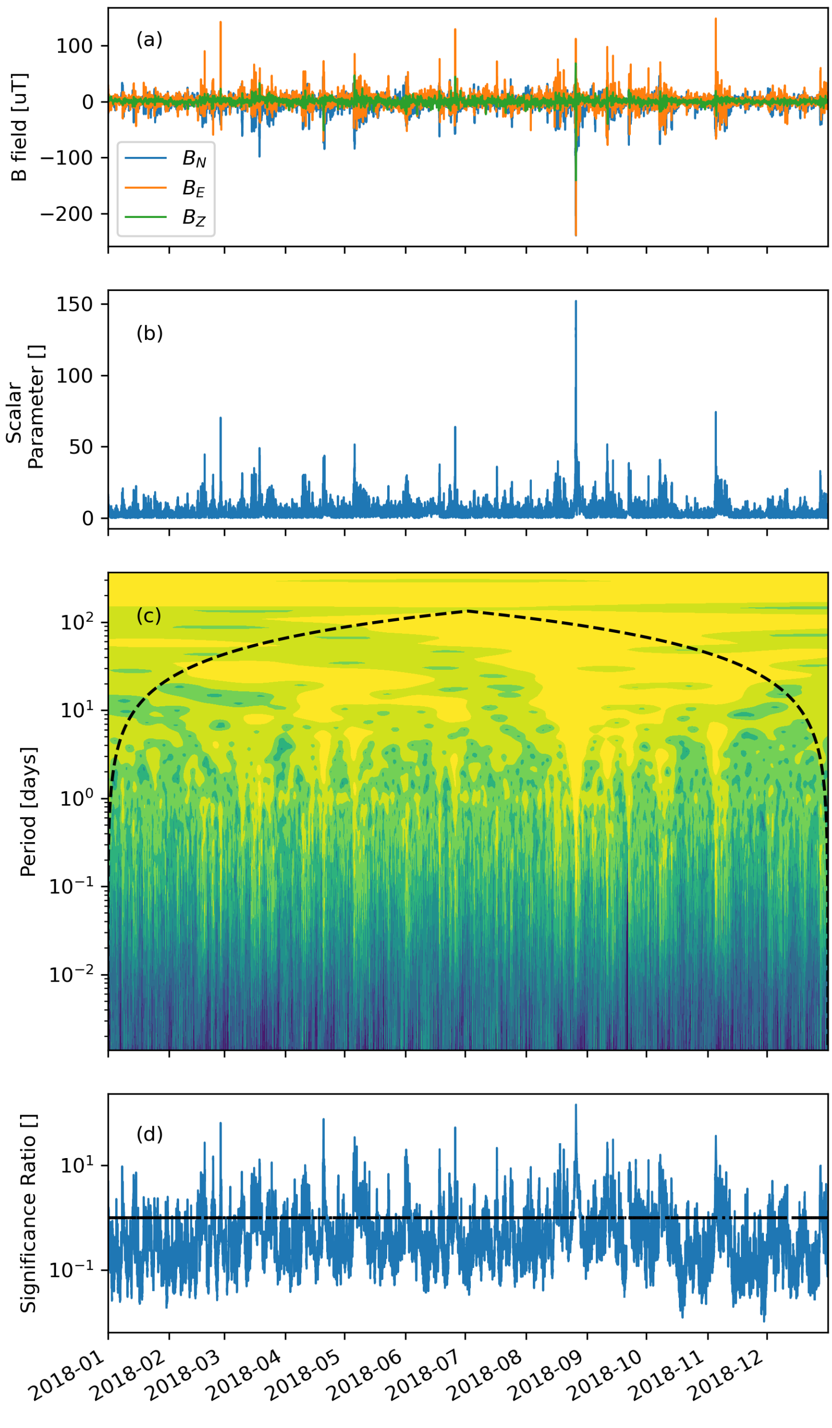

Figure 4. Example Wavelet analysis process: (a) B field at Boulder, CO magnetometer as a function of time. (b) Scalar parameter formed from B field. (c) Wavelet periodogram for the scalar parameter. Color indicates power. (d) Significance ratio for periods between 3 seconds and 3 days

end of the interval. The example analysis shown reveals a significant amount of power with a ∼20 day period from February to June, and a large event with significant power at all frequencies centered on August 26, when the largest Kp value (7+) for 2018 is observed.

Finally, the average significance ratio is computed as a function of time and shown in Fig. 4d. This is done by dividing the power (shown as color) by the expected power using a 95% confidence interval based on a red noise analysis (Gilman et al., 1963). This ratio is then averaged across periods from 3 seconds up to 3 days. The resulting average significance ratio is shown with a black line indicating the value of 1. Points above this line are interpreted as times with significant magnetic activity for the purposes of this study. The event in late August has as significance ratio of over 100, and can be traced back through the wavelets, s parameter, and B field.

The probability of each magnetometer station experiencing significant magnetic activity is shown as color in Fig. 5. There is a trend that equatorial stations close to water are the most active. This is because of three reasons - first, equatorial sites are the most sensitive to the equatorial electrojet (EEJ) (Appleton, 1946; Yamazaki & Maute, 2017). Second, in some areas proximity to water increases the variability of magnetic field data through the coast effect (Parkinson, 1959, 1962), where the vertical field perturbations is abnormally large and correlated to the onshore horizontal field. This effect is primarily driven by the difference in conductivity between the ground and the water. Lastly, magnetometers react strongly to ring current enhancements, which are strongest near the magnetic equator. The SuperMag network at equatorial latitudes has even been shown to react to auroral and cross-magnetotail currents (Newell & Gjerloev, 2012).

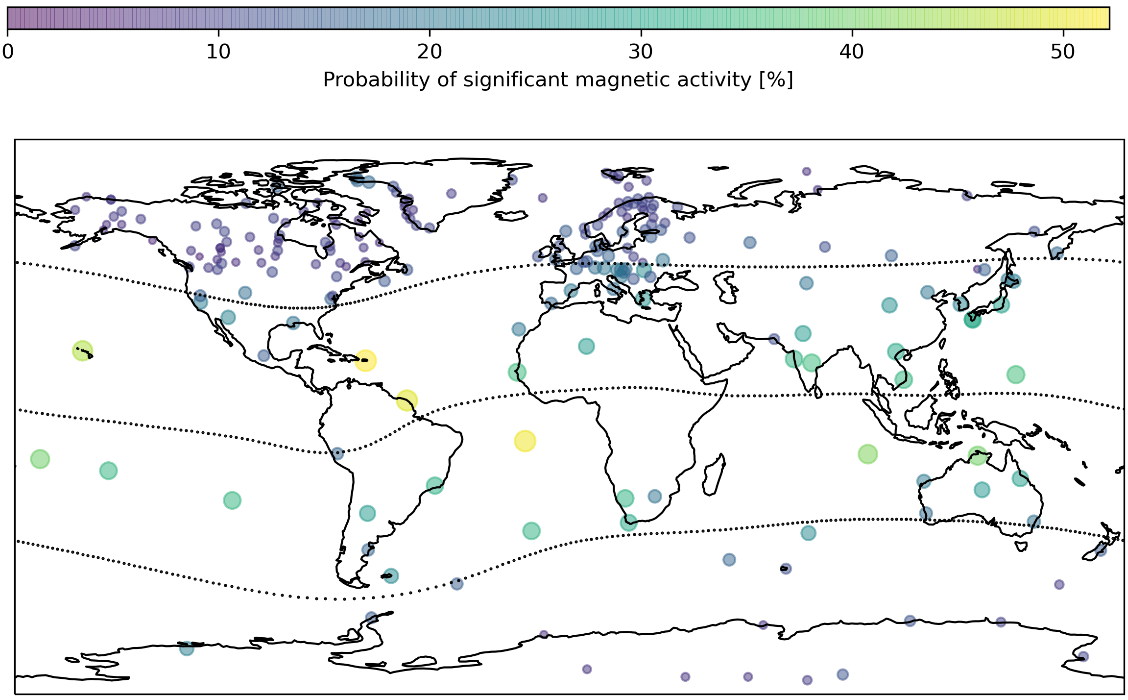

Figure 5. Map of probability of significant magnetic activity for all magnetometers in SuperMAG network. Dotted lines show -45, 0, 45 magnetic latitudes on the summer solstice, 2018.

The probability of magnetic activity is plotted as a function of the magnetic latitude in Fig. 6. A dashed line shows the median probability of magnetic activity in nine bins stretching from 0 to 90 degrees. The probability is highest at equatorial latitudes and slowly drops to a minimum near 70 degrees. Poleward of this, the probability of activity increases again.

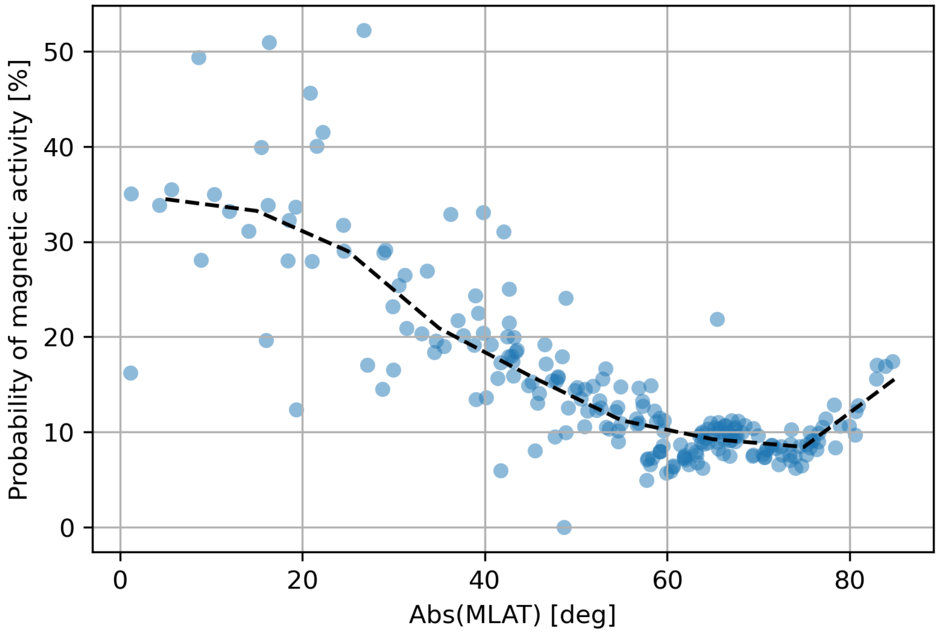

Figure 6. Probability of magnetic activity as a function of magnetic latitude.

Next, consider when in both time and MLT significant magnetic activity occurs. Another 2D histogram, very similar to Fig. 2, of time and MLT is shown in Fig. 7. There are a handful of strong magnetic events in this year as evidenced by the strong vertical yellow lines in Fig. 7a. Many of these are well-aligned with Kp, shown in Fig. 7c. The most prominent yellow line is centered around Aug 26, which also had the highest Kp value (7+) for all of 2018. Unlike the TVA data, the magnetic activity is spread across MLT for many of the storms because the SuperMAG stations are located across many longitudes.

The magnetic activity is typically highest in the late night and early morning which is where the majority of the magnetic activity is expected. Figure 7b shows a histogram of magnetic activity for each site with the magnetic latitude of the site shown as color. The average activity of all the magnetometers is shown as a dashed black line. From this plot, it looks like there are two populations of magnetometers - those that have their peak activity near magnetic midnight and those that have their peak activity probability near magnetic noon. All but one of the noon-peaking stations is equatorial (dark blue in color) which points to the EEJ and equatorial fountain effect as an explanation for some of this bi-modality.

To further investigate this phenomenon, the ratio of the average magnetic activity from 11 MLT to 13 MLT (noon activity) to the the average magnetic activity from 23 MLT to 1 MLT (midnight activity) as a function of magnetic latitude is shown in Fig. 8. The color and size of the points indicates the average activity for that site across all MLTs through the year.

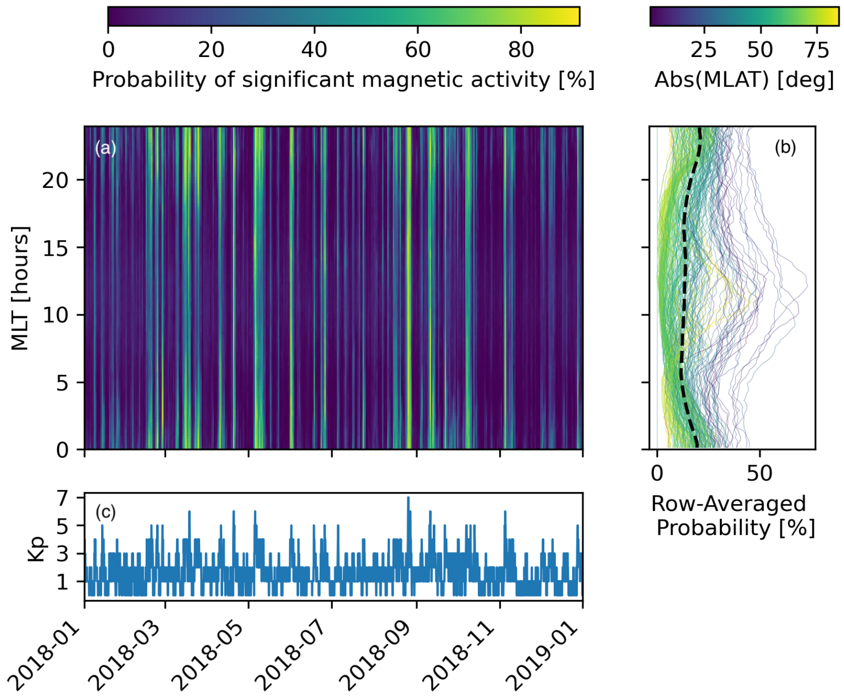

Figure 7. (a) Two dimensional histogram of magnetic activity probability as a function of time and MLT. (b) Row-averaged probability histograms just as a function of MLT for each magnetometer station. Color indicates magnetic latitude (c) K_P as a function of time.

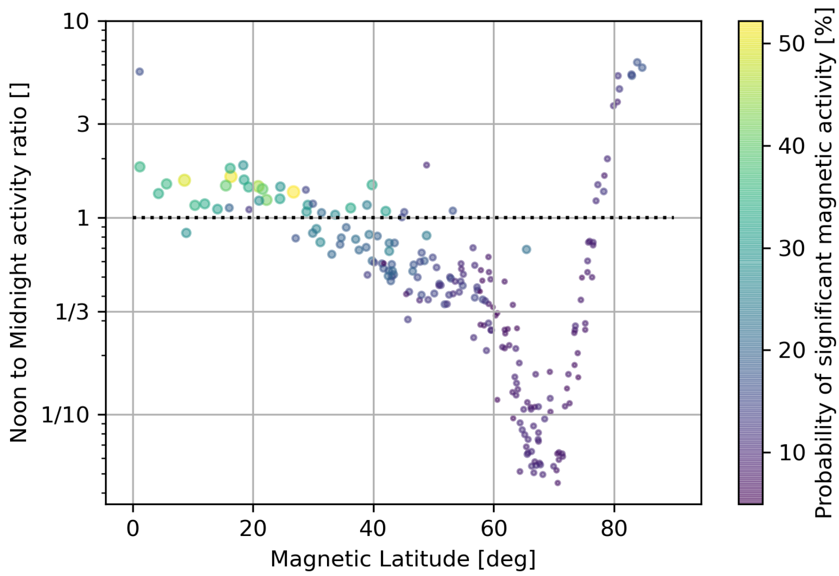

Figure 8. Ratio of noon (MLT between 11 and 13) activity to midnight (MLT between 23 and 1) activity as a function of magnetic latitude.

Confirming the trends observed in Fig. 6, equatorial sites are much more active as evidenced by the large yellow points at the left end of the spectrum in Fig. 8. There is also a clear decreasing trend in the noon to midnight ratio - indicating a preference for near-midnight magnetic activity - until a magnetic latitude near 70 degrees. At these high latitudes, near-midnight activity is more than 10 times more likely than near-noon activity. After this point, the trend reverses and the stations are much more likely to be active near local noon. This trend is also seen in (Ngwira et al., 2013) but with a transition magnetic latitude near 30-40 degrees. The lower transition to the cusp is likely due to Ngwira et al. only analyzing extreme events, when the auroral oval moves down to lower latitudes e.g. (Carbary, 2005).

4 Statistical Connections

To determine the connection between a given GIC measurement node - magnetometer pair, the amount of time during which there is magnetic activity at the magnetometer, a significant DC transient at the GIC measurement node, both a significant transient and magnetic activity, or neither a significant transient nor magnetic activity is used. Fig. 9 visualizes these times for four representative cases. In each diagram, the purple circle represents all the times with magnetic activity, and the beige circle represents all the times with significant transients. The intersection of the purple and beige circles (grey) shows times when there are both significant transients and magnetic activity. The large pink circle represents the entire year, of which the times with significant transients, magnetic activity, or both are included. The area in the pink circle not occupied by any other circle represents the amount of time that neither significant transients nor magnetic activity are observed. The counts (in thousands) for these subsets are also printed in the circles. Consider case (a); there are about 2.9 + 3.3 = 6.2 million instances of currents which exceeded the 2σ threshold for this GIC measurement node and 7.1 + 3.3 = 10.4 million cases of magnetic activity, 3.2 million of which are simultaneous. The total of all the numbers in each diagram gives the number of seconds in the year 2018.

Fig. 9a represents a strong connection - significant DC transients and magnetic activity often occur simultaneously. Fig. 9b shows a exemplary case of ”false positives” where magnetic activity is frequently recorded, but significant transients are not. For this case, there are more than 14 million occurrences of magnetic activity, but only 1.5 million significant transients. Fig. 9c shows an example of a false negative - where the magnetometer is not active even though there are many cases of the current exceeding the 2-σ QDC threshold. In this case, the magnetic activity only coincides with 640 thousand of the more than 5 million transients at this node. Lastly, Fig. 9d shows a pair that anti-correlates, significant transients are less likely at this node if magnetic activity is observed at the magnetometer.

This analysis can be used to calculate the probability multiplier for a given GIC measurement node - magnetometer pair. The probability multiplier is the ratio of the probability of a significant transient given magnetic activity to the unconditional probability of a significant transient. Using Bayes' law, this is given as:

$$PM = \frac{p(g|m)}{p(g)} = \frac{p(g \cap m)}{p(g)p(m)} \tag{3}$$

Where $p(g)$ is the probability of a significant DC transient, $p(m)$ is the probability of magnetic activity, and $p(g{\cap}m)$ is the probability of coincident magnetic activity and a 2-σ transient. If all current spikes are independent from magnetic activity, $p(g{\cap}m)$ would be equal to $p(g) \times p(m)$ and the probability multiplier would always be equal to 1. A probability multiplier greater than one indicates increased transient probability with magnetic activity.

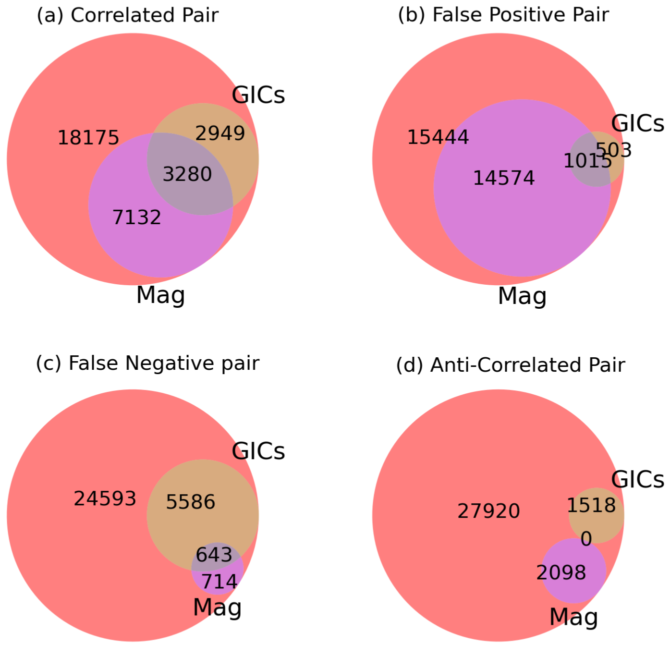

Figure 9. Venn diagrams for four representative magnetometer-GIC node pairs. In each diagram, the large salmon circles represent all times. Tan circles represent times where significant DC transients are observed, purple circles represent times where magnetic activity is observed, and the grey intersection represents times where both magnetic activity and significant DC transients are observed. Numbers in each sector count the total times for each condition.

Denoting the number of occurrences in a year of magnetic activity as N_M, the number of 2σ transients as N_G, the number of significant transients coincident with magnetic activity as N_B, and the total number of times (The number of seconds in 2018 - 31,536,000) as N_A, the probability multiplier is given by:

$$PM = \frac{N_A N_B}{N_G N_M} \tag{4}$$

As an example, the probability multiplier for the first pair in Fig. 9, is given by $\frac{31{,}536 \times 3{,}280}{10{,}412 \times 6{,}229} \approx 1.6$. The probability multiplier for each GIC measurement node - magnetometer pair is computed and shown in Fig. 10.

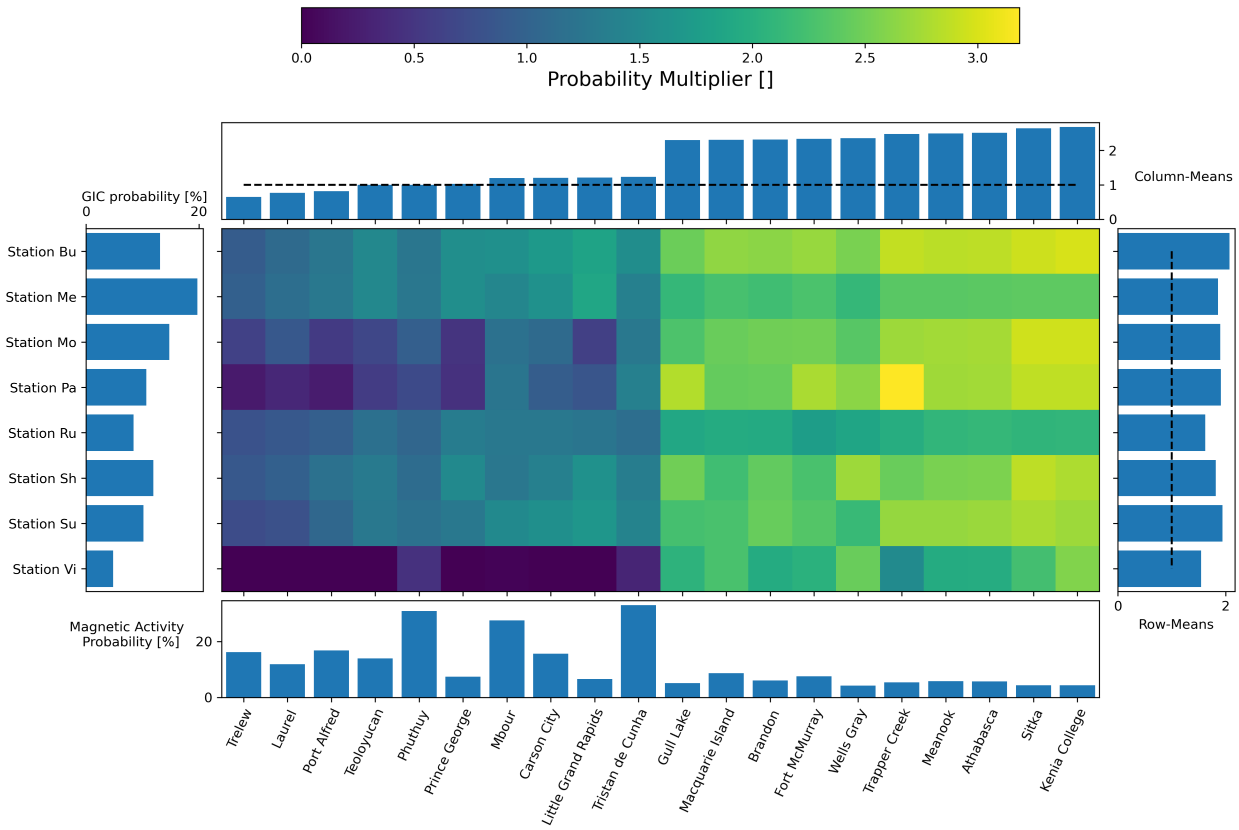

Figure 10. Probability multipliers for GIC node - magnetometer pairs with activity and DC transient probability means. See text for details.

The color in the center plot shows how much more probable a significant DC transient at the station shown on the y axis is if magnetic activity is observed at the magnetometer on on the x axis. For example, significant transients at Station Vi are more than three times more likely if magnetic activity is observed at Kenai College, AK. Only the 10 most influential and 10 least influential, as determined by the probability multiplier, magnetometers are shown. The row and column average of this matrix are shown in the top and right plots. The column averages (top) show the average influence of a given magnetometer across all GIC measurement nodes. The most influential station (Kenai College) has an average multiplier near 2.5, and the least influential station (Trelew, Argentina) has an average multiplier of just under 1. The row means (right) show the susceptibilities of a given station to all the magnetometers (not just the 20 shown). All the row means are significantly larger than 1, meaning that all of the stations are affected by space weather. The bottom plot shows the probability of magnetic activity at that station, and the left plot shows the probability of a significant DC transient at the given station. These subplots show the same information as presented in Fig. 5 and Fig. 3, respectively. The average probability multiplier for the entire matrix is just over 1.6 but for the best connected pairs it is higher than 3.

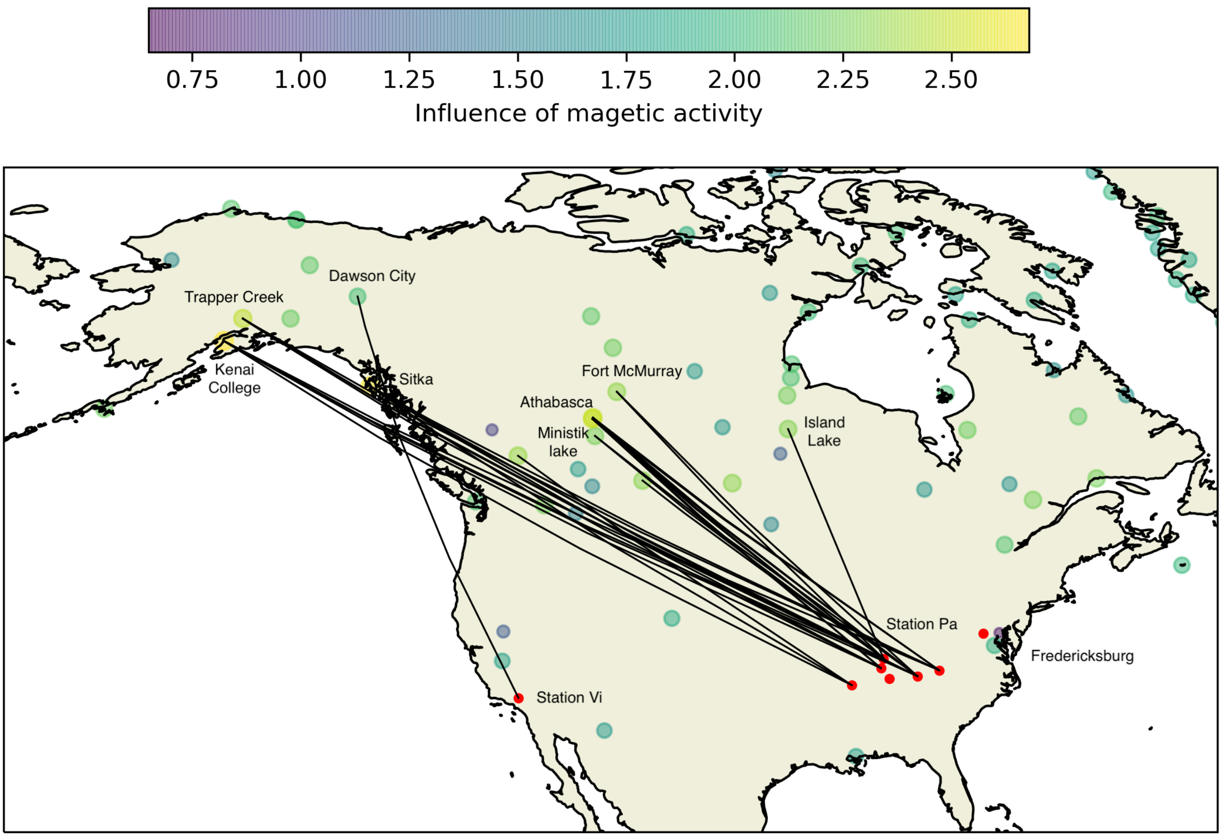

Figure 11. Map of strongest magnetometer-GIC node connections, color indicates average influence of magnetic activity for all GIC measurement nodes

These connections are also visualized through a map. The average influence of each magnetometer (top subplot in Fig. 10) is shown as color in Fig. 11. The 30 strongest connections are shown as thin black lines. The strongest connections, as indicated by the probability multiplier, are between GIC nodes and high-latitude sites in northern Canada and Alaska. In all of these connections, the magnetometer is to the West of the GIC measurement node. This may be due to the shape of the current flow in this region (Keiling et al., 2009).

Previous work (EPRI, 2020) has shown that magnetic fields correlate with measured currents well when the separation is less than 300 miles, but this correlation diminishes as the distance increases out to 700 miles. (EPRI, 2020)'s study is different from this work because of the way that a significant DC transient is defined by being more than 2 standard deviations above the average QDC level as opposed to a correlation-based analysis. Additionally, (EPRI, 2020) only considers storm-time and does not consider northern Canada or Alaska data. Many of the significant DC transients considered here are small, and therefore not a threat to the power grid.

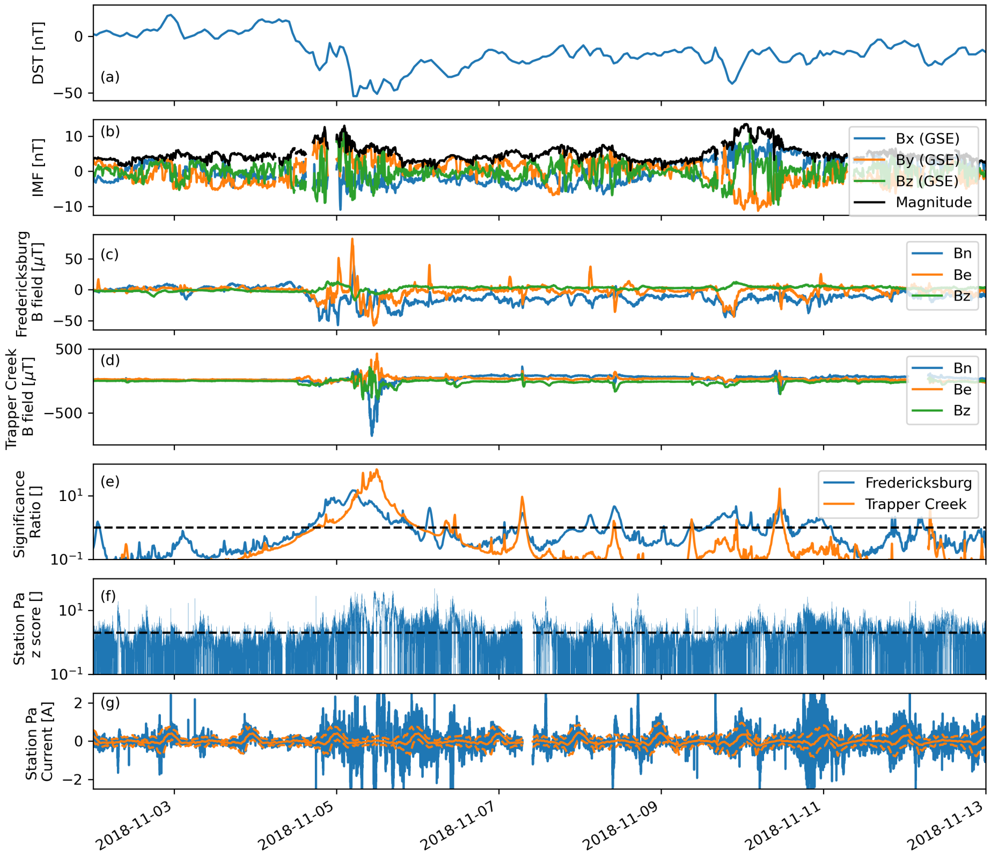

Figure 12. Time series for two magnetometers and Station Pa. (a) Disturbance Storm Time (DST) index. (b) Interplanetary Magnetic Field (IMF). (c) Magnetic field at Fredericksburg, close to the GIC measurement node. (d) Magnetic field at Trapper Creek, Alaska. (e) Significance ratio of both magnetometers (f) Z score of Station Pa current (g) Raw current with QDC and σ for Station Pa.

These probability multipliers are related to the original magnetometer and current data by examining time series for a well connected pair (as determined by this analysis) and a geographically close pair. The strongest connection in this analysis is between Station Pa and Trapper Creek (in Alaska) with probability multiplier of 3.18. The Fredericksburg magnetometer is much nearer to Station Pa, but it has a lower probability multiplier of 2.07. Magnetic activity at either of these magnetometers corresponds to higher DC transient probability at station Pa, but activity at Trapper creek is about 50% more indicative of a significant transient despite being much further away.

Figure 12 shows the disturbance storm time (DST) index in (a) and the interplanetary magnetic field (IMF) in (b). The raw data for both magnetometers are shown in (c) and (d), and the raw data for Station Pa shown in the bottom panel (g). The processed magnetometer data is shown in panel (e), and the processed current data is shown in panel (f). The B field at Trapper creek has much larger excursions relative to quiet time variability than Fredericksburg. The magnitude of the quiet time variability at Trapper Creek is near 50 nT and the spikes are larger than 500 nT (a factor of 10). At Fredericksburg, the quiet time variability is near 20 nT and the spikes are near 50 nT (a factor of 2.5). The effective signal to noise ratio is approximately 4 times higher at Trapper Creek than at Fredericksburg. The larger spikes at Trapper Creek also mean that the significance ratio is lower at quiet times, as can be seen in between the 7th and 11th in Fig. 12c. This makes the processed Trapper creek significance ratio more indicative of significant DC transients because of the fewer false positive errors.

Just the day of November 6th, 2018 is shown in Fig. 13. Rather than the B fields, the magnitude of the horizontal B field rate $\sqrt{\frac{dB_N}{dt}^2 + \frac{dB_E}{dt}^2}$ is shown to follow (EPRI, 2017). Neither of the two B field rates match the station current, but the Trapper Creek B field rate is closer.

Notably, there is an enhancement near 3 UT in the Fredericksburg B field rate that does not appear in the Station Pa current. All three datasets show activity near 11 UT, but the shape of the current is closer to Trapper Creek than it is to Fredericksburg, which shows a single spike. Lastly, there is activity near 22 UT in both magnetic datasets that is not reflected in the current. The magnetic activity at Trapper Creek that is coincident with current enhancements at station Pa (11 UT) is larger than the activity that does not (3 and 22 UT), which makes it easy to pick out. However, the magnetic activity at Fredericksburg which is coincident with current enhancements at station Pa (11 UT) is smaller than the activity which does not coincide with current enhancements (3 and 22 UT). These three events, centered at 3, 11, and 22 UT show a similar trend to Fig. 12 - that the magnetic activity which has an effect on the current stands out more prominently from the background noise.

5 Conclusion

This paper offers a glimpse into what can be done with network analysis in the space sciences - particularly with the connection between space weather as evidenced by magnetometer measurements and deviations from the expected currents. The analysis of current data reveals a trend of higher probability of a significant DC transient in the early morning MLT sector. However, this is more dramatic at some stations than others. The magnetometer analysis showed that the equatorial and coastal magnetometers are the most active due to the combination of the coast effect, Equatorial ElectroJet, and ring current enhancements. The latitude also drives the ratio of noon-to-night activity with equatorial sites being more active near local noon and high latitude sites being more active near midnight. This trend is reversed near the auroral boundary. Probabilistic analysis shows which magnetometers are the most indicative of significant DC transients in the power grid, and where they are located. Three key points emerge from this analysis:

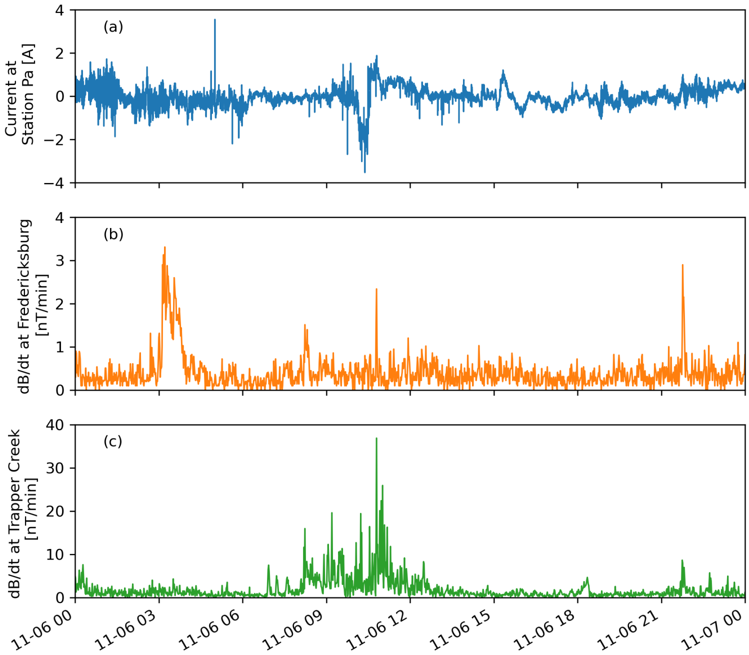

Figure 13. Time series for two magnetometers and Station Pa. (a) Current at station Pa (b) dB/dt at Fredericksburg, close to the GIC measurement node. (c) dB/dt at Trapper Creek, Alaska.

- Significant DC transients are, on average, 1.6 times more likely to occur when there is statistically significant magnetic activity.
- This analysis indicates that magnetometers far from the GIC nodes can possibly provide a better indication of significant DC transients.
- Without any prior knowledge of the physical system, the network analysis technique presented in this paper is able to identify a strong connection between significant DC transients occurring at mid-latitude stations, and a set of auroral and sub-auroral magnetometers that, in all likelihood, reflect the occurrence of substorm-related ionospheric currents. While the physics of this connection are not yet fully identified, it is nevertheless clear that this analysis provides a means of estimating the likelihood of significant DC transients. As such, this represents a significant step forward in space weather effects forecasting for GICs.

Future work could continue the network analysis of the magnetometer data to study the temporal and spatial extent of storms and sub-storms. A valuable next step for this work would be to study which magnetometers are the best indicators of *future* DC transients. Additional GIC data from northern Canada and Alaska would enable further investigation into the trend reported here that significant transients preferentially connect with magnetometers in northern Canada and Alaska rather than with magnetometers nearby.

Acknowledgments

The data provided for this study are part of the Sunburst network. We are currently not able to release the GIC data directly, due to agreements with EPRI and the power utilities who provided data for this analysis, however, we have posted the simulation results and GIC-QDC data on `https://zenodo.org`. We gratefully acknowledge the SuperMAG collaborators (`https://supermag.jhuapl.edu/info/?page=acknowledgement`) for the indices employed in this study available at `https://supermag.jhuapl.edu/indices`. We acknowledge use of NASA/GSFC's Space Physics Data Facility's OMNIWeb service, and OMNI data available at `https://omniweb.gsfc.nasa.gov`.

References

Appleton, E. V. (1946). Two anomalies in the ionosphere. *Nature*, *157*(691). doi: https://doi.org/10.1038/157691a0

Boccaletti, S., Latora, V., Moreno, Y., Chavez, M., & Hwang, D.-U. (2006). Complex networks: Structure and dynamics. *Physics Reports*, *424*(4), 175 - 308. Retrieved from `http://www.sciencedirect.com/science/article/pii/S037015730500462X` doi: https://doi.org/10.1016/j.physrep.2005.10.009

Boteler, D., & Pirjola, R. (2017, January). Modeling geomagnetically induced currents. *AGU Space Weather*, *15*, 258-276. doi: doi:10.1002/2016SW001499

Boteler, D. H. (2019). A 21st Century View of the March 1989 Magnetic Storm. *Space Weather*, *17*. doi: 10.1029/2019SW002278

Camporeale, E. (2019). The challenge of machine learning in space weather: Nowcasting and forecasting. *Space Weather*, *17*(8), 1166-1207. Retrieved from `https://agupubs.onlinelibrary.wiley.com/doi/abs/10.1029/2018SW002061` doi: https://doi.org/10.1029/2018SW002061

Carbary, J. F. (2005). A kp-based model of auroral boundaries. *AGU Space Weather*, *3*(10). doi: https://doi.org/10.1029/2005SW000162

Dods, J., Chapman, S., & Gjerloev, J. (2017). Characterizing the ionospheric current pattern response to southward and northward imf turnings with dynamical supermag correlation networks. *Journal of Geophysical Research (Space Physics)*, *122*, 1883– 1902. doi: doi:10.1002/2016JA023686

Dods, J., Chapman, S. C., & Gjerloev, J. W. (2015). Network analysis of geomagnetic substorms using the supermag database of ground-based magnetometer stations. *Journal of Geophysical Research: Space Physics*, *120*(9), 7774-7784. Retrieved from https://agupubs.onlinelibrary.wiley.com/doi/abs/10.1002/2015JA021456 doi: 10.1002/2015JA021456

Donges, J. F., Zou, Y., Marwan, N., & Kurths, J. (2009, AUG). The backbone of the climate network [Article]. *EPL*, *87*(4). doi: {10.1209/0295-5075/87/48007}

EPRI. (2017, October). *Space weather activity and the impact on the transmission system observed in september 2017* (Tech. Rep. No. 3002011973). Palo Alto, CA: Electric Power Research Institute.

EPRI. (2018a, June). *Node installation.* Supplemental Project Notice.

EPRI. (2018b, July). *Sunburst network membership.* Supplemental Project Notice.

EPRI. (2020, March). *Improving conductivity models for geomagnetically induced current (gic) estimation* (Tech. Rep. No. 3002017897). Palo Alto, CA: Electric Power Research Institute.

Gilman, D. L., Fuglister, F. J., & Mitchell, J., J. M. (1963, 03). On the Power Spectrum of "Red Noise". *Journal of the Atmospheric Sciences*, *20*(2), 182-184. Retrieved from https://doi.org/10.1175/1520-0469(1963)020<0182:OTPSON>2.0.CO;2 doi: 10.1175/1520-0469(1963)020⟨0182:OTPSON⟩2.0.CO;2

Gjerloev, J. W. (2009). A global ground-based magnetometer initiative. *Eos, Transactions American Geophysical Union*, *90*(27), 230-231. Retrieved from https://agupubs.onlinelibrary.wiley.com/doi/abs/10.1029/2009EO270002 doi: 10.1029/2009EO270002

Keiling, A., Angelopoulos, V., Runov, A., Weygand, J., Apatenkov, S. V., Mende, S., ... Auster, H. U. (2009). Substorm current wedge driven by plasma flow vortices: Themis observations. *Journal of Geophysical Research: Space Physics*, *114*(A1). Retrieved from https://agupubs.onlinelibrary.wiley.com/doi/abs/10.1029/2009JA014114 doi: https://doi.org/10.1029/2009JA014114

Lanzerotti, L. J. (2001). Space Weather Effects on Technologies. *In Song D., Singer H.J and Siscoe G.L. Space Weather. AGU Geophysical Monograph 125*, 11-22.

Lesher, R. L., Porter, J. W., & Byerly, R. T. (1994). Sunburst - a network of gic monitoring systems. *IEEE Transactions on Power Delivery*, *9*(1), 128 - 137. doi: 10.1109/61.277687

Malik, N., Bookhagen, B., Marwan, N., & Kurths, J. (2011). Analysis of spatial and temporal extreme monsoonal rainfall over south asia using complex networks. *Climate Dynamics*, *39*(3-4), 971–987. doi: 10.1007/s00382-011-1156-4

McGranaghan, R. M., Bhatt, A., Matsuo, T., Mannucci, A. J., Semeter, J. L., & Datta-Barua, S. (2017). Ushering in a new frontier in geospace through data science. *Journal of Geophysical Research: Space Physics*, *122*(12), 12,586-12,590. Retrieved from https://agupubs.onlinelibrary.wiley.com/doi/abs/10.1002/2017JA024835 doi: 10.1002/2017JA024835

Milgram, S. (1967). The small-world problem. *Psychology Today*, *1*(1), 60-67. doi: 10.1037/e400002009-005

Newell, P. T., & Gjerloev, J. W. (2012). Supermag-based partial ring current indices. *Journal of Geophysical Research: Space Physics*, *117*(A5). Retrieved from https://agupubs.onlinelibrary.wiley.com/doi/abs/10.1029/2012JA017586 doi: https://doi.org/10.1029/2012JA017586

Ngwira, C. M., Pulkkinen, A., Wilder, F. D., & Crowley, G. (2013). Extended study of extreme geoelectric field event scenarios for geomagnetically induced current applications. *AGU Space Weather*, *11*, 121-131. doi: doi:10.1002/swe.20021

Orr, L., Chapman, S. C., & Gjerloev, J. W. (2019). Directed network of substorms using supermag ground-based magnetometer data. *Geophysical Research Letters*, *46*, 6268– 6278. doi: https://doi.org/10.1029/2019GL082824

Parkinson, W. D. (1959). Directions of rapid geomagnetic fluctuations. *The Geo-*

physicsal Journal of the Royal Astronomical Society, *2*(1).
Parkinson, W. D. (1962). The influence of continents and oceans on geomagnetic variations. *Geophysical Journal International*.
Pirjola, R. (2000). Geomagnetically induced currents during magnetic storms. *IEEE Trans. Plasma Sci.*, *28*(6), 1867-1873.
Pirjola, R. (2002). Review on the calculation of the surface electric and magnetic fields and geomagnetically induced currents in ground based technological systems. *Surveys in Geophysics*, *23*, 71-90.
Pulkkinen, A., Bernabeu, E., Thomson, A., Viljanen, A., Pirjola, R., Boteler, D., ... MacAlester, M. (2017). Geomagnetically induced currents: Science, engineering, and applications readiness. *Space Weather*, *15*(7), 828-856. Retrieved from `https://agupubs.onlinelibrary.wiley.com/doi/abs/10.1002/2016SW001501` doi: 10.1002/2016SW001501
Schrijver, C. J., Kauristie, K., Aylward, A. D., Denardini, C. M., Gibson, S. E., Glover, A., ... Vilmer, N. (2015). Understanding space weather to shield society: A global road map for 2015–2025 commissioned by COSPAR and ILWS. *Advances in Space Research*, *55*(12), 2745 - 2807. Retrieved from `http://www.sciencedirect.com/science/article/pii/S0273117715002252` doi: https://doi.org/10.1016/j.asr.2015.03.023
Steinhaeuser, K., Ganguly, A. R., & Chawla, N. V. (2011). Multivariate and multiscale dependence in the global climate system revealed through complex networks. *Climate Dynamics*, *39*(3-4), 889–895. doi: 10.1007/s00382-011-1135-9
Torrence, C., & Compo, G. (1998). A practical guide to wavelet analysis. *Bulletin of the American Meterological Society*, *79*(1). doi: https://doi.org/10.1175/1520-0477(1998)079⟨0061:APGTWA⟩2.0.CO;2
Tsonis, A. A., Swanson, K. L., & Roebber, P. J. (2006, 05). What Do Networks Have to Do with Climate? *Bulletin of the American Meteorological Society*, *87*(5), 585-596. Retrieved from `https://doi.org/10.1175/BAMS-87-5-585` doi: 10.1175/BAMS-87-5-585
Viljanen, A., & Pirjola, R. (1994). Geomagnetically induced currents in the Finnish high-voltage power system. *Surveys in Geophysics*, *15*, 383-408.
Yamazaki, Y., & Maute, A. (2017). Sq and eej—a review on the daily variation of the geomagnetic field caused by ionospheric dynamo currents. *Space Science Reviews*, *206*. doi: 5DOI:10.1007/s11214-016-0282-z